Composites Science and Technology 227 (2022) 109614

Contents lists available at ScienceDirect

Composites Science and Technology

journal homepage: www.elsevier.com/locate/compscitech

Novel approach for damage detection in multiscale CNT-reinforced composites via wireless Joule heating monitoring

Xoan F Sánchez-Romate *, Carlos González, Alberto Jiménez-Suárez, Silvia G. Prolongo

Materials Science and Engineering Area, Escuela Superior de Ciencias Experimentales y Tecnología, Universidad Rey Juan Carlos, Calle Tulipán s/n, 28933, Móstoles, Madrid, Spain

ARTICLE INFO

Keywords:
Glass fibres
Smart materials
Thermomechanical properties
Non-destructive testing

ABSTRACT

A novel method for strain and crack propagation monitoring based on Joule heating capabilities of multiscale carbon nanotube reinforced glass fiber composites (GFRP-CNT) is reported. The manufactured GFRP-CNT composites show good Joule heating capabilities with heating rates ranging from 3 to 56 °C min^{-1} at applied voltages from 30 to 105 V, respectively. Multiscale GFRP-CNT composites present similar tensile strength and Young's Modulus than conventional GFRP but very enhanced failure strain due to the toughening effect of CNTs. The wireless monitoring via Joule heating shows a very high sensitivity and strain resolution (with values ranging from 0.01 to 0.1%) for early crack initiation and subsequent propagation. Finally, the thermal IR imaging also allows to create a complete mapping of the health of the structure during the whole test, allowing the detection, localization and quantification of early damage and, thus, proving an outstanding potential for Structural Health Monitoring (SHM) applications in comparison to other conventional techniques.

1. Introduction

Nowadays, there is an increasing effort in the development of polymer-based composite materials due to the interesting combination of properties in comparison to the conventional structural metallic alloys. In this regard, the use of glass fiber reinforced plastics (GFRPs) is gaining attention in applications such as wind turbine blades [1,2], marine industry [3] or in biomedicine [4].

However, one of the main limitations of fiber reinforced plastics (FRPs) is the variety and complexity of failure modes, such as matrix cracking, fiber breakage or interfacial debonding. In this regard, for a proper characterization of these complex failure modes, there is an arising interest in the development of multiple inspection techniques based on Lamb waves [5], fiber Bragg grating sensors (FBGs) [6] or by magnetic detection modes [7].

Moreover, the use of carbon nanoparticles is now of interest, as they exhibit very interesting mechanical and physical properties [8–10]. Also, the presence of conductive carbon nanoparticle networks inside an insulating thermosetting matrix, promotes an enhancement of the electrical conductivity due to their intrinsic conductive properties, as well as the tunneling effect occurring between adjacent nanoparticles [11–13]. The latter effect, jointly with their inherent piezoresistivity, makes them very suitable for Structural Health Monitoring (SHM) applications based on the change of electrical conductivity when subjected to strain or damage. In fact, they present very promising properties as wearable sensors for human motion [14–17] or as capacitive sensors for pressure monitoring [18,19] due to their excellent sensitivity to strain and damage detection [20,21]. More specifically, very high values (above 50) of Gauge Factor (GF), defined as the change of the normalized resistance divided by the applied strain have been reported in comparison to other conventional techniques, such as metallic gauges with values around 2–3 [22,23].

Furthermore, the addition of carbon nanoparticles also provides other interesting functionalities. For example, the use of carbon nanotubes (CNTs) and graphene has proven to be a very efficient solution for resistive heating due to Joule's effect [24–28]. More specifically, their excellent Joule's heating capabilities have been exploited for the development of de-icing systems [29], shape-memory activation [30] and for a thermoelectrical triggering of curing and post-curing processes [31]. Moreover, it is well known that the heating induced by Joule's effect is proportional to the electrical conductivity of the composite [32].

In this regard, the resistive heating capabilities of GFRP-CNT multiscale composites have been widely used mainly for *in-situ* curing to

* Corresponding author.
E-mail address: xoan.fernandez.sanchezromate@urjc.es (X. F Sánchez-Romate).

https://doi.org/10.1016/j.compscitech.2022.109614
Received 8 April 2022; Received in revised form 25 May 2022; Accepted 24 June 2022
Available online 28 June 2022

facilitate the manufacturing process or for composite repairs [33,34]. Here, the rapid thermal response to resistive heating (less than 30 s to reach 150 °C from room temperature), promotes an adequate homogenization during curing [34].

Therefore, this work aims to combine both the piezoresistive properties and Joule's heating capabilities of CNT reinforced polymers for strain and damage monitoring of GFRP composites. In fact, the SHM of GFRP structures reinforced with CNTs has been widely explored by means of electrical measurements, proving excellent capabilities for strain and damage monitoring [35,36]. However, the main limitation of the conventional electrical resistance-based monitoring techniques is that they do not offer enough information about the location and quantification of damage. In order to partially solve this problem, Electrical Impedance Tomography (EIT) has proved to be a good technique for damage detection as they offer a complete mapping of the structure [37,38]. Nevertheless, this technique involves the setting of often complicated electrode's networks connected to a monitoring system, thus, requiring the use of complex mathematical and statistical tools to properly evaluate the electrical measurements.

On the other hand, Joule's heating activation does not require such a complex design of electrodes and the temperature reached on the sample can be easily mapped by using an IR camera, which would act as a wireless non-contact monitoring system. Here, the changes in the electrical conductivity due to strain or the presence of a damage can be easily reflected in changes in the heating capabilities of the material.

Therefore, this study reports the use of Joule's heating as an on-line strain and damage monitoring system in GFRP-CNT multiscale composites made of ±45 oriented non-crimp fabrics. Different voltage levels were applied to evaluate the temperature effect on the mechanical performance and thermoelectrical sensitivity. Very high strain resolutions were reported prior to crack initiation (from 0.01% at 120 °C to 0.1% at 40 °C) and early crack formation and propagation was successfully monitored, giving a complete information about location and damage extent.

2. Experimental

2.1. Materials

The epoxy resin was an *Araldite LY556* with a XB3473 amino hardener, both supplied by *Sigma Aldrich*. Multi-walled carbon nanotubes (MWCNTs) were *NC7000*, supplied by *Nanocyl*, with an average diameter of 9.5 nm and a length up to 1.5 μm. The reinforcement was an E-glass fiber, supplied by *Resinas Castro*, with a layer sequence of $[\pm 45]_{4s}$. The E-glass fiber was X600E05A-45/45 biaxial fabric with an areal weight of 300 g/m^2 per layer.

2.2. Manufacturing process

The GFRP-CNT multiscale composites were fabricated by manual hand lay-up. First, MWCNTs were dispersed in the epoxy matrix by means of three roll milling process by following a seven-steps cycle with a progressive reduction of the adjacent rolls, as shown in Table 1, with a constant speed of the last roll of 250 rpm. The MWCNT weight fraction was set as 0.2 wt% as it is far above the percolation threshold of the system [39]. In addition, three-roll milling was selected as dispersion technique as the shear forces induced by the rotating rolls promote an adequate dispersion of the CNTs [40]. After dispersion process, the CNT/epoxy mixture was degassed under vacuum conditions at 80 °C for 15 min. Then, the hardener was added in a proportion monomer to hardener of 100 to 23. Finally, after manual hand lay-up, the multiscale composites were cured at 140 °C for 8 h [41] in a hot press at a pressure of 0.6 MPa [42].

Table 1
Three-roll milling parameters for CNT dispersion into the epoxy matrix.

Cycle	GAP 1 (μm)	GAP 2 (μm)
1	120	40
2	75	25
3	45	15
4–7	15	5

2.3. Characterization of multiscale composites

The microstructural characterization was carried out by means of Field Emission Gun-SEM (FEG-SEM), using a *Nova NanoSEM* module in the fracture surfaces of multiscale composites. Previously, the samples were coated by a thin layer of platinum for a better characterization. Heating-cooling curves by Joule's effect were characterized by increasing the applied voltage between two electrodes made of copper wire and attached with silver ink, using a *Chroma programmable DC power supply Model 62012P-600-8*. The temperature reached in the samples was recorded by a thermal IR camera from *FLIR Tools* with a thermal resolution of 0.1 °C.

2.4. Tensile tests via Joule heating monitoring

The multiscale GFRP-CNT composites were subjected to tensile tests by following the ASTM D3039 with simultaneous thermal monitoring via Joule heating at six initial temperatures: room temperature (20 °C), 40, 60, 80, 100 and 120 °C. These temperatures were selected far below the glass transition temperature of the epoxy system, which was determined in other studies above 170 °C [43]. For this purpose, three samples were tested for each temperature condition. Their dimensions were $100 \times 20 \times 3$ mm^3. The test rate was fixed at 0.5 mm min^{-1} in every case and the current passing through the sample was recorded every 30 s. Prior to start the test, the initial temperature was maintained in each sample for 10 min to guarantee a proper heating homogenization. It is important to point out that the samples used for the heating-cooling characterization by Joule's effect were not the same than those used for the SHM tests but presented the same laying sequence, dimensions, and CNT content. In these tests, the camera was placed at 0.25 m of the specimens, near its minimum focal distance, to get a thermal mapping with high resolution.

3. Results and discussion

3.1. Characterization of multiscale GFRP composites

The mechanical performance of GFRP-CNT multiscale and reference composites is summarized by representative stress-strain curves in Fig. 1a. It can be noticed that the addition of CNTs into the epoxy matrix has two main effects. On one side, it promotes a slight reduction of both Young's Modulus and Tensile Strength when compared to the reference samples (7171 ± 137 to 6650 ± 157 MPa and 136.6 ± 1.2 to 132.1 ± 3.5 MPa, for the neat and CNT reinforced samples, respectively). This slight reduction of mechanical properties with the addition of CNTs may be attributed to the higher viscosity of the mixture in comparison to neat epoxy [44]. Therefore, the resin flow could be lower, thus, leading to a higher resin fraction [45]. In fact, the average thickness of the CNT-reinforced samples was 3.35 mm whereas in case of neat samples was 3.24 mm. On the other hand, it induces a significant increase of the failure strain, that is, the strain level where the crack initiates (6.40 ± 0.32 to 9.35 ± 0.74%, for the neat and CNT reinforced samples, respectively). This is explained by the toughening effect of the CNTs, which promotes a slowing crack initiation and propagation in the GFRP composites, due to their crack-bridging properties in a similar way that the observed in similar multiscale composites [46]. In this regard, the microstructural characterization of the samples by FEG-SEM analysis shows a very homogeneous CNT distribution inside the epoxy matrix (Fig. 1b and c), with the absence of prevalent aggregates, being an

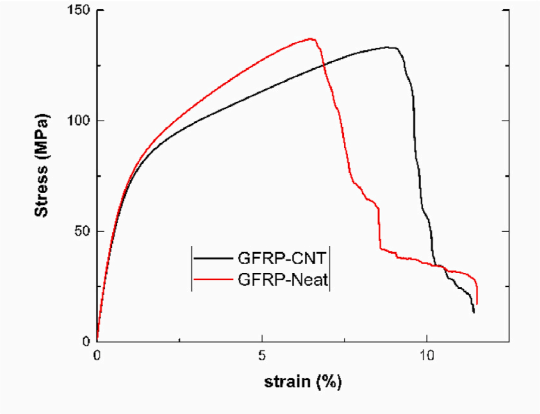

(a)

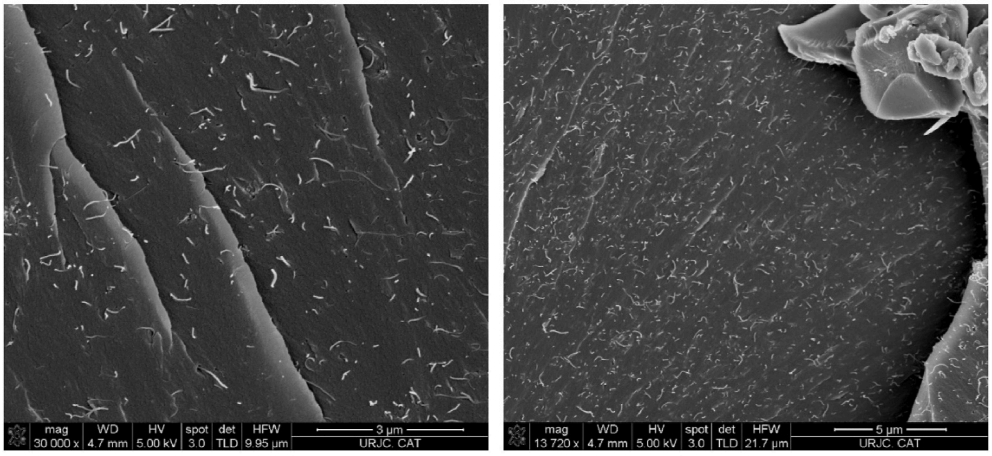

(b) (c)

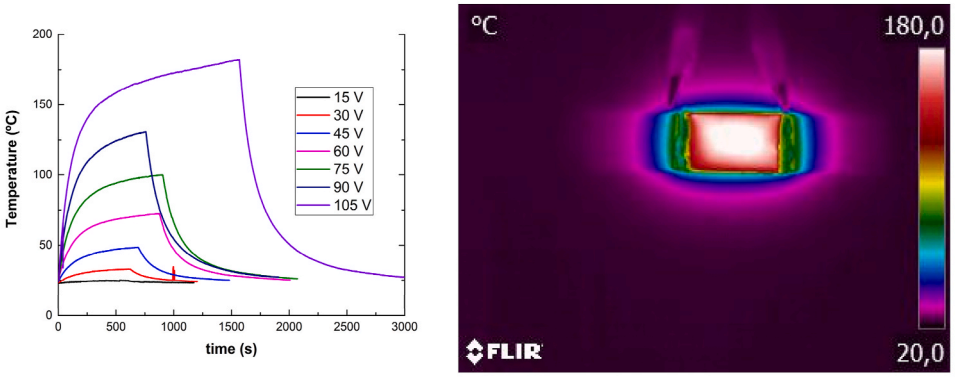

(d) (e)

Fig. 1. (a) Stress-strain curves of GFRP-CNT and GFRP-neat resin composites, (b) and (c) FEG-SEM images of the fracture surfaces indicating the homogeneous CNT dispersion throughout the matrix; (d) heating-cooling curves via Joule Effect for different applied voltages and (e) IR image of temperature distribution during resistive heating.

indicative of the effectiveness of the dispersion procedure. Therefore, it can be concluded that the CNT addition does not promote a significant detriment of the mechanical properties of the GFRPs in terms of strength and stiffness. It even leads to significant increase of the toughness.

Furthermore, the Joule heating capabilities of GFRP-CNT composites are shown in the heating-cooling curves summarized in Fig. 1d. Here, it can be observed, as expected, that the increasing applied voltage between the two electrodes promotes an increase of the temperature reached at the stable condition.

Moreover, by analyzing in detail the heating-cooling curves, it can be noticed that the increasing voltage also induces higher heating-cooling rates in the first stages of the Joule heating tests. More specifically, the heating rates vary from 3 to 56 °C min^{-1} at applied voltages from 30 to 105 V, respectively, during the first minute of heating. Furthermore,

the cooling rates are slightly slower and vary from −2.8 to −50 °C min^{-1} at applied voltages from 30 to 105 V, respectively, during the first minute of cooling. This is explained by the well-known Joule's law:

$$Q = V \bullet I \bullet t$$

where Q is the heat flow in a time *t*, *V* the applied voltage and *I* the measured current.

In this regard, the increasing applied voltage leads to an increase of the current passing through the specimen (as observed in the *V–I* curves of Fig. S1) and, thus, to a higher heat flow during the transient heating of the samples, explaining the higher heating-cooling rates with the increasing applied voltage. In addition, it can be pointed out that the samples subjected to a higher applied voltage take more time to reach a stable temperature profile (from 5 to more than 20 min at applied voltages from 30 to 105 V, respectively). This can be explained by the higher heat exchange with the environment.

Furthermore, it can be also observed that the heating is very homogeneous in the sample (Fig. 1e) for every applied voltage (Fig. S2) with a maximum temperature deviation of 15 °C in the samples reaching an average quasi-stable temperature of 180 °C (that is, those subjected to 105 V) as it is observed in the graphs of Fig. S3. Therefore, it can be concluded that the developed GFRP-CNT multiscale composites have very good Joule heating capabilities with a homogenous temperature distribution. In this context, their capabilities for strain and damage monitoring via Joule resistive heating are going to be explored.

3.2. Analysis of temperature profile during mechanical testing

Fig. 2a illustrates an example of the correlation between the mechanical performance and the temperature profile in a centered region of a specimen. Here, it can be observed that the temperature decreases throughout the mechanical test, as expected, due to the decrease of the electrical conductivity of the sample during the test, reducing the effectiveness of the Joule's heating mechanism. This detriment is associated to two main effects: on the one hand, the increase of the tunneling resistance between adjacent CNTs due to the applied strain, reflected in a soft decrease of the temperature, and, on the other hand, the breakage of conductive pathways due to the crack initiation and subsequent propagation until failure, reflected in a sudden temperature decrease (Fig. 2b). The first effect dominates the behavior of the sample at the beginning of the test whereas the latter prevails in the last stages, coinciding with the sudden drop of the mechanical load (highlighted area of Fig. 2a). In this regard, the first stages would be useful to determine the thermal sensitivity of the system to strain whereas the last stages would give the thermal sensitivity to crack propagation.

In this regard, Fig. 2c shows the temperature variation for the different tested conditions. It can be stated that the initial temperature reached in the sample plays a fundamental role in the thermoelectrical behavior of the samples during the test. More specifically, it may play a crucial role in the thermal sensitivity (TS) of the system, which can be calculated for the different conditions from the temperature profile prior to crack initiation.

It is known that, accordingly to Joule's law, the heat applied and, therefore, the temperature reached depends on the external applied

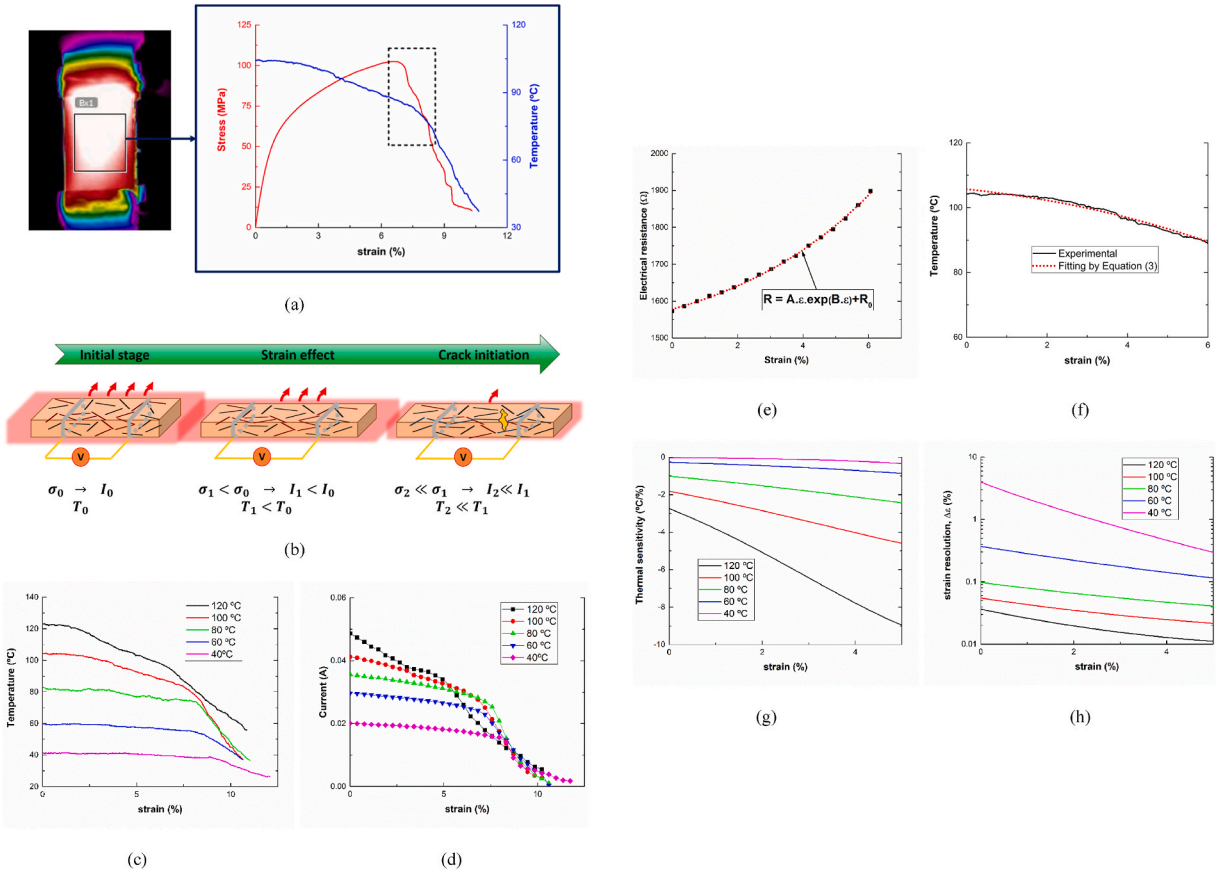

Fig. 2. a) Example of a tensile curve with the corresponding temperature variation (the highlighted dashed square refers to the early stages of crack propagation), b) schematics of how Joule heating is correlated to the electrical conductivity during a monitoring test where the red arrows indicate the heat flow and the voltage is applied between two electrodes; c) temperature profiles and d) measured current for the different tested conditions; e) electrical resistance measured and fitted by Equation (2), f) comparison between measured temperature at low strain levels and by fitting using Equation (3), g) thermal sensitivity and h) strain resolution for the different tested conditions calculated by Equations (4) and (5), respectively.

voltage and the electrical resistance, following the next expression:

$$T \propto \frac{V^2}{R} \tag{1}$$

Where T is the temperature reached, V is the external applied voltage and R is the intrinsic electrical resistance of the sample.

As commented before, the electrical resistance changes with applied strain because of the prevalent role of tunneling transport mechanisms and it can be estimated from the current measurements carried out during the test, shown in the graph of Fig. 2d, at strain levels prior to crack initiation, as the applied voltage remains constant during the entire test. Accordingly to Ohm's law, $R = V/I$, so it is easy to determine the dependence of the electrical resistance with applied strain (Fig. 2e). In this context, it is known that the tunneling resistance follows a linear-exponential relationship with the tunneling distance between adjacent carbon nanoparticles [47] and, thus:

$$R = A\varepsilon \bullet \exp(B\varepsilon) + R_0 \tag{2}$$

where A and B are two constants and R_0 the initial electrical resistance of the sample.

By combining Equations (1) and (2), it is easy to obtain a relationship between the temperature of the sample and the applied strain:

$$T = \frac{1}{C\varepsilon \bullet \exp(D\varepsilon) + E} \tag{3}$$

where, C, D and E are fitting parameters from the experimental measurements.

It can be observed that the expression of Equation (3) fits the temperature variation during the first stages of the tensile test as observed in a representative example given in Fig. 2f.

Therefore, the thermal sensitivity can be obtaining by deriving Equation (3):

$$TS = \frac{dT}{d\varepsilon} = \frac{-C \bullet \exp(D\varepsilon) - C\varepsilon \bullet D \bullet \exp(D\varepsilon)}{(C\varepsilon \bullet \exp(D\varepsilon) + E)^2} \tag{4}$$

Fig. 2g shows the thermal sensitivity estimated for the different tested conditions by fitting the experimental measurements. It can be stated that the TS increases with the initial temperature reached in the sample, as expected, due to the increasing heating power. In addition, from the thermal resolution of the IR camera, which is $\Delta T = -0.1$ °C, it is also possible to obtain the minimum value of strain that can be detected, that is, the strain resolution of the system, $\Delta\varepsilon$:

$$\frac{\Delta T}{\Delta \varepsilon} = TS \quad \rightarrow \Delta\varepsilon = \frac{\Delta T}{TS} \tag{5}$$

In this context, Fig. 2h shows the strain resolution for each condition depending on the strain level of the sample. It can be observed that, at low strains ($\varepsilon \sim 0.5\%$), $\Delta\varepsilon$ is around 0.031% at 120 °C, 0.049% at 100 °C, 0.088% at 80 °C, 0.32% at 60 °C and 2.89% at 40 °C. The strain resolution at high temperatures, thus, is very high, proving an outstanding sensitivity of the system, however, at lower heating

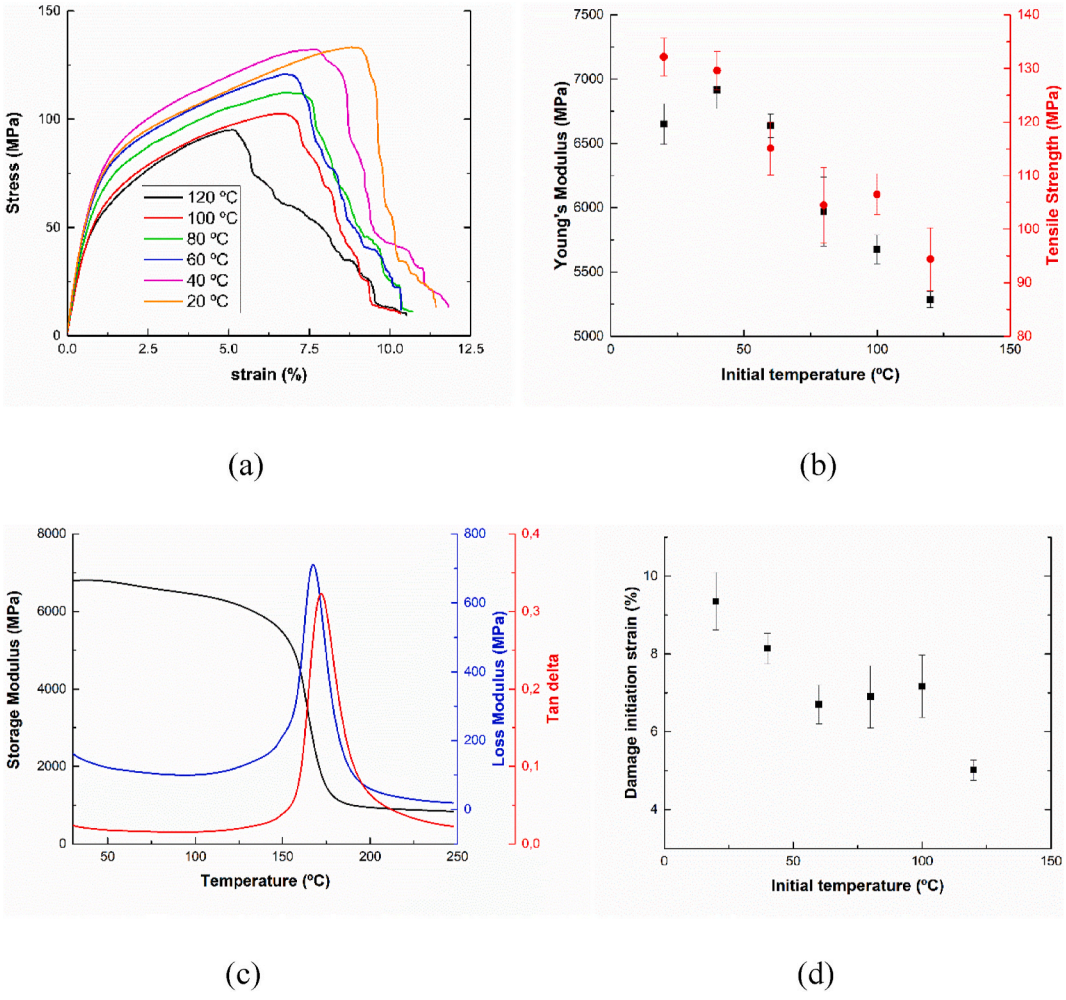

Fig. 3. a) Stress-strain curves for the different tested conditions, b) Young's Modulus and Tensile Strength of specimens as a function of initial temperature, c) DMTA curve of the GFRP-CNT sample and d) strain values at early crack initiation.

temperatures, the resolution is very low for small strain levels. However, the crack initiation does not take place in the very first stages of the tensile test, so it is necessary to further explore the thermomechanical behavior of the samples.

3.2.1. Temperature effect on mechanical properties

In this regard, for a deeper analysis, Fig. 3a shows the mechanical behavior of the samples for each condition. The aim is to analyze the temperature effect on the mechanical performance and to correlate it with the temperature variation in order to demonstrate the capabilities of Joule's heating monitoring for early damage detection.

Accordingly, it can be observed that the increasing temperature of the samples leads to a reduction of the Young's Modulus (Fig. 3b), which is more prevalent at 100 and 120 °C heated samples. This behavior is in good agreement with the thermomechanical results from DMTA tests (Fig. 3c) where a reduction of the storage modulus is observed with increasing temperature due to the softening of the matrix. Here, it can be observed that, at the temperature range of the resistive heating tests, there are no significant variations of the loss modulus and the values of tanδ are very low. This implies that the viscoelastic properties are not very prevalent at this range and, thus, no significant delay between the mechanical load and the strain are expected. Furthermore, the values of the Tensile Strength also decrease with increasing temperature (Fig. 3b) as the rising temperature weakens the bonding capability and stress transfer efficiency of GFRP/epoxy interfaces [48,49]. In addition, it is important to point out that, although there is a reduction in the mechanical performance at 40 and 60 °C, it is not so prevalent when comparing to the non-heated samples, whose results are also reported in Fig. 3a (orange curve), indicating that the Joule's heating monitoring does not significantly compromise the mechanical performance of the sample at low heating power values.

Furthermore, Fig. 3d also shows the strain values corresponding to the early drop of the mechanical load, which indicates the failure initiation of the laminate. Here, it can be observed that the strain values generally decrease with increasing temperature. This is an indicative of a later crack initiation with decreasing temperature. These results are in good agreement with the previous statement about the weakening effect of temperature in the bonding capability of the interface epoxy/GF [48, 49], thus, leading an earlier interfacial failure and, therefore, an earlier crack initiation. However, from the stress-strain curves (Fig. 3a), it can be elucidated that the crack propagation takes places in a more sudden way at lower temperatures, with a more drastic drop of the mechanical response. This is explained by the higher stiffness of the epoxy matrix, promoting a much more rigid response and, thus, a sudden crack propagation.

In addition, the strain resolution at early crack initiation can be estimated from Equation (5) at the strain values summarized in Fig. 3d. Here, the calculated values for the strain resolution are 0.01% for 120 °C, 0.018% for 100 °C, 0.036% for 80 °C, 0.095% for 60 °C and 0.1% for 40 °C. Therefore, in every case, the system presents a very high sensitivity for early damage detection with very low values of strain resolution, proving a very high sensitivity in comparison to other studies [50]. It would demonstrate the efficiency of wireless monitoring via Joule's Effect for early damage detection even at low heating power levels, where the mechanical performance of the laminates is not significantly compromised.

3.2.2. Analysis of damage evolution via temperature profile

Here, to further explore the damage mechanisms in this type of materials and even the performance and scope of Joule's heating monitoring proposed, Fig. 4a summarizes the evolution of the strain and damage monitoring during the tensile test via IR thermal camera imaging and its correlation to the mechanical performance and temperature profile for the different conditions (Fig. 4b and c). It can be observed that the system is totally able to detect the early crack initiation at every temperature (point 4 of IR images). As commented before, the crack

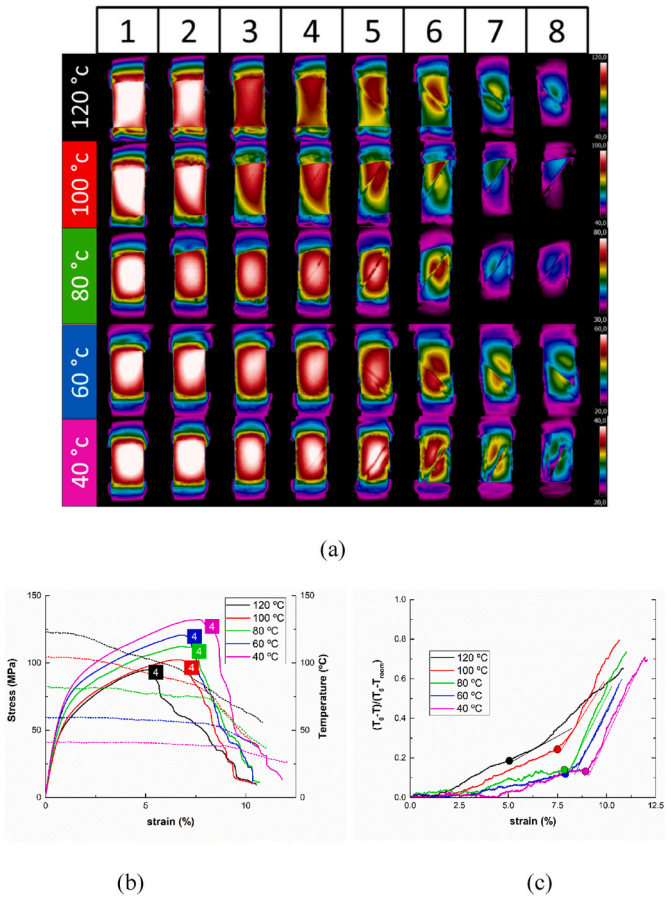

Fig. 4. a) Thermal IR images showing the evolution of the damage in the samples during the tensile test, b) thermomechanical profile and c) variation of normalized temperature for the different tested conditions.

propagation promotes a sudden disruption of the electrical network that is reflected in a sudden loss of electrical conductivity and, thus, in a prominent decrease of the measured current, as previously observed in Fig. 2d. This sudden decrease of electrical conductivity is not uniform in the sample, being more prevalent in the areas where the disruption of electrical pathways is more significant. Therefore, this disruption is reflected in a more significant temperature decrease in the damaged areas in comparison to the pristine ones. For these reasons, this method allows to have a complete mapping of crack propagation during the test (points 5 to 8 of IR images).

Furthermore, by comparing the IR mapping and the normalized temperature, T_N profile, estimated from the initial temperature of the sample, T_0 and the room temperature, T_{room}, that is $T_N = (T_0 - T)/(T_0 - T_{rom})$, it can be noticed that the temperature decrease during crack propagation is more prevalent in the case of low initial temperature conditions (Fig. 4c), due to a more rapid crack propagation, as stated before in the mechanical analysis. More specifically, the samples at 120 °C, which exhibited the slowest crack propagation, also showed the lowest relative variation of the temperature after damage initiation (black curve of Fig. 4c). Therefore, although the samples at 40 °C showed the lowest thermal sensitivity prior to crack initiation, it showed the highest one once crack propagates, whereas the samples at 120 °C showed the opposite behavior.

Furthermore, from the thermal mapping of the samples, it is possible to estimate the damage extent. In this regard, Fig. 5 shows the crack evolution in two different cases: the first one, which is correlated to a crack propagation in a localized area (Movie S1), being reflected in a sudden temperature decrease in the damaged region (Fig. 5a) but a less drastic decrease of the global average temperature of the sample due to

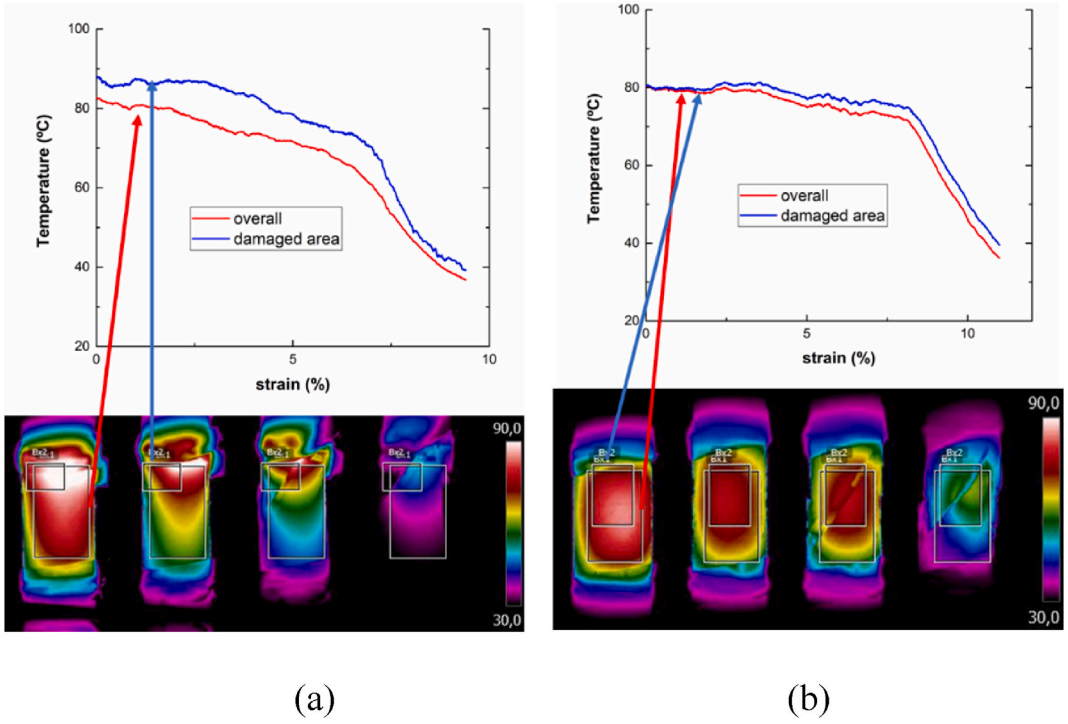

Fig. 5. Temperature profiles of the overall specimen and the damaged area for a) a localized and b) a more global crack propagation during the tensile test.

the localized nature of the damage. In addition, there is a significant difference between the average temperature of the overall temperature of the sample and the temperature in the region where crack initiates. On the other hand, the second case refers to an overall crack propagation through the central region of the specimen (Movie S2). Here, the temperature profiles of both the damaged region and the overall sample exhibit a similar behavior due to the global nature of the damage (Fig. 5b). Therefore, this method can give a very detailed information about how damage initiates in the specimens as well as the way it propagates, helping to better understand the crack propagation mechanisms in this type of materials.

Supplementary video related to this article can be found at https://doi.org/10.1016/j.compscitech.2022.109614

In any case, the proposed novel method provides detection and localization of early damage and quantification of damage extent via thermal mapping, proving the outstanding capabilities of Joule's heating activation for SHM purposes over other conventional non-destructive testing (NDT) techniques, where such a detailed information is not often easily obtained. In addition, the experimental setup is very simple as it does not involve the design of a complex electrical network of electrodes in the sample or the use of complex mathematical and statistical tools. This method only requires the simple position of electrodes to induce Joule's heating, using a common and inexpensive IR camera as a wireless and non-contact sensor. Therefore, this novel method gives both overall and detailed information of the health of the structure with a very high sensitivity, allowing registering IR structure mappings.

4. Conclusions

Joule heating capabilities of multiscale GFRP-CNT composites have been explored for developing a novel method based on a wireless monitoring of strain and early crack propagation.

The manufactured GFRP-CNT composites showed interesting Joule's effect capabilities with heating rates ranging from 3 to 56 °C min^{-1} at applied voltages from 30 to 105 V, respectively. Moreover, the mechanical performance is not compromised by the addition of CNTs with only a slight reduction of the tensile strength and Young's Modulus and highly enhanced failure strain in comparison to the neat reference samples.

The wireless monitoring by means of Joule heating activation have proved a very high thermal sensitivity prior to crack initiation, reaching values of strain resolution of around 0.01–0.1%. This sensitivity decreased with decreasing initial temperature. Furthermore, a successfully early crack initiation and subsequent propagation has been achieved by means of thermal IR imaging, allowing to have a complete mapping of the structure without the need of a complex electrode disposition and statistical tools for the proper interpretation of the results.

Therefore, the proposed novel method for SHM of composite materials shows an enormous potential and applicability in comparison to other conventional techniques based on the electrical resistance monitoring as they would allow a rapid characterization by thermal mapping without the needing of a complex electrode network, with a high defect resolution.

CRediT roles

Xoan F. Sánchez-Romate: Conceptualization; Formal analysis; Methodology; Visualization; Writing – original draft **Carlos González:** Formal analysis; Methodology **Alberto Jiménez-Suárez:** Supervision; Writing – review and editing **Silvia G. Prolongo:** Funding acquisition; Writing – review and editing.

Declaration of competing interest

The authors declare that they have no known competing financial interests or personal relationships that could have appeared to influence the work reported in this paper.

Acknowledgements

This work was supported by the Ministerio de Economía y Competitividad of Spanish Government [PID2019-106703RB-I00].

Appendix A. Supplementary data

Supplementary data to this article can be found online at https://doi.org/10.1016/j.compscitech.2022.109614.

References

[1] G. Santo, M. Peeters, W. Van Paepegem, J. Degroote, Dynamic load and stress analysis of a large horizontal axis wind turbine using full scale fluid-structure interaction simulation, Renew. Energy 140 (2019) 212–226.

[2] K. Pender, L. Yang, Regenerating performance of glass fibre recycled from wind turbine blade, Compos. B Eng. 198 (2020), 108230.

[3] N.H. Nash, A. Portela, C.I. Bachour-Sirerol, I. Manolakis, A.J. Comer, Effect of environmental conditioning on the properties of thermosetting- and thermoplastic-matrix composite materials by resin infusion for marine applications, Compos. B Eng. 177 (2019), 107271.

[4] S. Shabahang, S. Kim, S. Yun, Light-guiding biomaterials for biomedical applications, Adv. Funct. Mater. 28 (24) (2018), 1706635.

[5] H. Duflo, B. Morvan, J. Izbicki, Interaction of Lamb waves on bonded composite plates with defects, Compos. Struct. 79 (2) (2007) 229–233.

[6] O. Rifaie-Graham, E.A. Apebende, L.K. Bast, N. Bruns, Self-reporting fiber-reinforced composites that mimic the ability of biological materials to sense and report damage, Adv. Mater. 30 (19) (2018), 1705483.

[7] M.D. Crall, S.G. Laney, M.W. Keller, Multimodal damage detection in self-sensing fiber reinforced composites, Adv. Funct. Mater. 29 (12) (2019), 1806634.

[8] M.F. Yu, O. Lourie, M.J. Dyer, K. Moloni, T.F. Kelly, R.S. Ruoff, Strength and breaking mechanism of multiwalled carbon nanotubes under tensile load, Science 287 (5453) (2000) 637–640.

[9] L. Ci, S. Sreekala, O. Nalamasu, J. Suhr, P.M. Ajayan, P. Victor, X. Zhang, Fatigue resistance of aligned carbon nanotube arrays under cyclic compression, Nat. Nanotechnol. 2 (7) (2007) 417–421.

[10] M.F. De Volder, S.H. Tawfick, R.H. Baughman, A.J. Hart, Carbon nanotubes: present and future commercial applications, Science 339 (6119) (2013) 535–539.

[11] N. Hu, Y. Karube, M. Arai, T. Watanabe, C. Yan, Y. Li, Y. Liu, H. Fukunaga, Investigation on sensitivity of a polymer/carbon nanotube composite strain sensor, Carbon 48 (3) (2010) 680–687.

[12] Y. Liao, K. Mustonen, S. Tulic, V. Skakalova, S.A. Khan, P. Laiho, Q. Zhang, C. Li, M.R.A. Monazam, J. Kotakoski, H. Lipsanen, E.I. Kauppinen, Enhanced tunneling in a hybrid of single-walled carbon nanotubes and graphene, ACS Nano 13 (10) (2019) 11522–11529.

[13] L. Duan, D.R. D'hooge, L. Cardon, Recent progress on flexible and stretchable piezoresistive strain sensors: from design to application, Prog. Mater. Sci. 114 (2020), 100617.

[14] M. Amjadi, K. Kyung, I. Park, M. Sitti, Stretchable, skin-mountable, and wearable strain sensors and their potential applications: a review, Adv. Funct. Mater. 26 (11) (2016) 1678–1698.

[15] L. Zhang, K.S. Kumar, H. He, C.J. Cai, X. He, H. Gao, S. Yue, C. Li, R.C. Seet, H. Ren, Fully organic compliant dry electrodes self-adhesive to skin for long-term motion-robust epidermal biopotential monitoring, Nat. Commun. 11 (1) (2020) 1–13.

[16] S. Wang, Y. Fang, H. He, L. Zhang, C. Li, J. Ouyang, Wearable stretchable dry and self-adhesive strain sensors with conformal contact to skin for high-quality motion monitoring, Adv. Funct. Mater. (2020), 2007495.

[17] Q. Zheng, J. Lee, X. Shen, X. Chen, J. Kim, Graphene-based wearable piezoresistive physical sensors, Mater. Today 36 (2020) 158–179.

[18] Z. Tang, S. Jia, C. Zhou, B. Li, 3D printing of highly sensitive and large-measurement-range flexible pressure sensors with a positive piezoresistive effect, ACS Appl. Mater. Interfaces 12 (25) (2020) 28669–28680.

[19] J. Xu, H. Wang, T. Ma, Y. Wu, R. Xue, H. Cui, X. Wu, Y. Wang, X. Huang, W. Yao, A graphite nanoplatelet-based highly sensitive flexible strain sensor, Carbon 166 (2020) 316–327.

[20] M. Al-Bahrani, A. Cree, Micro-scale damage sensing in self-sensing nanocomposite material based CNTs, Compos. B Eng. 205 (2021), 108479.

[21] G. Yang, X. Feng, W. Wang, Q. OuYang, L. Liu, Z. Wu, Graphene and carbon nanotube-based high-sensitive film sensors for in-situ monitoring out-of-plane shear damage of epoxy composites, Compos. B Eng. 204 (2021), 108494.

[22] M. Qu, Y. Qin, Y. Sun, H. Xu, D.W. Schubert, K. Zheng, W. Xu, F. Nilsson, Biocompatible, flexible strain sensor fabricated with polydopamine-coated nanocomposites of nitrile rubber and carbon black, ACS Appl. Mater. Interfaces 12 (37) (2020) 42140–42152.

[23] X. Zhou, X. Zhang, H. Zhao, B.P. Krishnan, J. Cui, Self-healable and recyclable tactile force sensors with post-tunable sensitivity, Adv. Funct. Mater. 30 (38) (2020), 2003533.

[24] L. Huang, N. Yi, Y. Wu, Y. Zhang, Q. Zhang, Y. Huang, Y. Ma, Y. Chen, Multichannel and repeatable self-healing of mechanical enhanced graphene-thermoplastic polyurethane composites, Adv. Mater. 25 (15) (2013) 2224–2228.

[25] M.M. Shulaker, G. Hills, R.S. Park, R.T. Howe, K. Saraswat, H.P. Wong, S. Mitra, Three-dimensional integration of nanotechnologies for computing and data storage on a single chip, Nature 547 (7661) (2017) 74–78.

[26] J.L. Bento, E. Brown, S.J. Woltornist, D.H. Adamson, Thermal and electrical properties of nanocomposites based on self-assembled pristine graphene, Adv. Funct. Mater. 27 (1) (2017), 1604277.

[27] L. Wang, D. Wang, Z. Wu, J. Luo, X. Huang, Q. Gao, X. Lai, L. Tang, H. Xue, J. Gao, Self-derived superhydrophobic and multifunctional polymer sponge composite with excellent Joule heating and photothermal performance for strain/pressure sensors, ACS Appl. Mater. Interfaces 12 (11) (2020) 13316–13326.

[28] L. Vertuccio, F. Foglia, R. Pantani, M.D. Romero-Sánchez, B. Calderón, L. Guadagno, Carbon nanotubes and expanded graphite based bulk nanocomposites for de-icing applications, Compos. B Eng. 207 (2021), 108583.

[29] O. Redondo, S.G. Prolongo, M. Campo, C. Sbarufatti, M. Giglio, Anti-icing and de-icing coatings based Joule's heating of graphene nanoplatelets, Compos. Sci. Technol. 164 (2018) 65–73.

[30] M. Loeblein, A. Bolker, Z.L. Ngoh, L. Li, E. Wallach, S.H. Tsang, M. Pawlik, R. Verker, N. Atar, I. Gouzman, E.H.T. Teo, Novel timed and self-resistive heating shape memory polymer hybrid for large area and energy efficient application, Carbon 139 (2018) 626–634.

[31] B. Shi, Y. Shang, P. Zhang, S. Liu, S. Huang, B. Sun, B. Gu, K. Fu, Rapid electrothermal-triggered flooded thermoset curing for scalable carbon/polymer composite manufacturing, Compos. Sci. Technol. 200 (2020), 108409.

[32] A. Jiménez-Suárez, J. Martín-González, X.F. Sánchez-Romate, S.G. Prolongo, Carbon nanotubes to enable autonomous and volumetric self-heating in epoxy/polycaprolactone blends, Compos. Sci. Technol. 199 (2020), 108321.

[33] B. Mas, J.P. Fernández-Blázquez, J. Duval, H. Bunyan, J.J. Vilatela, Thermoset curing through Joule heating of nanocarbons for composite manufacture, repair and soldering, Carbon 63 (2013) 523–529.

[34] X. Xu, Y. Zhang, J. Jiang, H. Wang, X. Zhao, Q. Li, W. Lu, In-situ curing of glass fiber reinforced polymer composites via resistive heating of carbon nanotube films, Compos. Sci. Technol. 149 (2017) 20–27.

[35] S. Gao, R. Zhuang, J. Zhang, J. Liu, E. Mäder, Glass fibers with carbon nanotube networks as multifunctional sensors, Adv. Funct. Mater. 20 (12) (2010) 1885–1893.

[36] M. Al-Bahrani, A. Cree, A simple criterion to evaluate the degree of damage in composite materials after sudden impact loads by exploiting the MWCNTs piezoresistive property, Carbon 150 (2019) 505–517.

[37] T.N. Tallman, S. Gungor, K.W. Wang, C.E. Bakis, Tactile imaging and distributed strain sensing in highly flexible carbon nanofiber/polyurethane nanocomposites, Carbon 95 (2015) 485–493.

[38] H. Dai, E.T. Thostenson, Large-area carbon nanotube-based flexible composites for ultra-wide range pressure sensing and spatial pressure mapping, ACS Appl. Mater. Interfaces 11 (51) (2019) 48370–48380.

[39] X.F. Sánchez-Romate, J. Artigas, A. Jiménez-Suárez, M. Sánchez, A. Güemes, A. Ureña, Critical parameters of carbon nanotube reinforced composites for structural health monitoring applications: empirical results versus theoretical predictions, Compos. Sci. Technol. 171 (2019) 44–53.

[40] A. Jimenez-Suarez, M. Campo, M. Sanchez, C. Romon, A. Urena, Influence of the functionalization of carbon nanotubes on calendering dispersion effectiveness in a low viscosity resin for VARIM processes, Compos. B Eng. 43 (8) (2012) 3482–3490.

[41] A. Moisala, Q. Li, I.A. Kinloch, A.H. Windle, Thermal and electrical conductivity of single- and multi-walled carbon nanotube-epoxy composites, Compos. Sci. Technol. 66 (10) (2006) 1285–1288.

[42] K. Zhang, Y. Gu, M. Li, S. Wang, Z. Zhang, Effects of curing time and de-molding temperature on the deformation of glass fiber/epoxy resin prepreg laminates fabricated by rapid hot press, Polym. Polym. Compos. 27 (6) (2019) 301–313.

[43] S. Prolongo, R. Moriche, A. Jiménez-Suárez, M. Sánchez, A. Ureña, Advantages and disadvantages of the addition of graphene nanoplatelets to epoxy resins, Eur. Polym. J. 61 (2014) 206–214.

[44] M. Kasraie, P. Pour Shahid Saeed Abadi, Additive manufacturing of conductive and high-strength epoxy-nanoclay-carbon nanotube composites, Addit. Manuf. 46 (2021), 102098.

[45] X.F. Sánchez-Romate, A.D. Bosque, J. Artigas-Arnaudas, B.K. Muñoz, M. Sánchez, A. Ureña, A proof of concept of a structural supercapacitor made of graphene coated woven carbon fibers: EIS study and mechanical performance, Electrochim. Acta 370 (2021), 137746.

[46] X.F. Sánchez-Romate, A. Alvarado, A. Jiménez-Suárez, S.G. Prolongo, Carbon nanotube reinforced poly (ε-caprolactone)/Epoxy blends for superior mechanical and self-sensing performance in multiscale glass fiber composites, Polymers 13 (18) (2021) 3159.

[47] N. Hu, Y. Karube, C. Yan, Z. Masuda, H. Fukunaga, Tunneling effect in a polymer/carbon nanotube nanocomposite strain sensor, Acta Mater. 56 (13) (2008) 2929–2936.

[48] Y. Li, W. Li, J. Shao, Y. Deng, H. Kou, J. Ma, X. Zhang, X. Zhang, L. Chen, Z. Qu, Modeling the effects of interfacial properties on the temperature dependent tensile strength of fiber reinforced polymer composites, Compos. Sci. Technol. 172 (2019) 74–80.

[49] Y. Li, W. Li, J. Ma, S. Zheng, Z. Zhao, M. Yang, P. Dong, L. Chen, Temperature dependent longitudinal tensile strength model of unidirectional fiber reinforced polymer composites considering the effect of matrix plasticity, Extreme Mech. Lett. 40 (2020), 100963.

[50] D. Zhang, S. Xu, X. Zhao, W. Qian, C.R. Bowen, Y. Yang, Wireless monitoring of small strains in intelligent robots via a Joule heating effect in stretchable graphene–polymer nanocomposites, Adv. Funct. Mater. 30 (13) (2020), 1910809.